

## Space System Environment Interactions Investigation

M.J. Mandell  
G.A. Jongeward  
V.A. Davis  
I. Katz  
R. A. Kuharski

Maxwell Federal Division, Inc.  
Maxwell Technologies, Inc.  
8888 Balboa Avenue  
San Diego, CA 92123-1506

January 1998

Final Report  
December 1991-December 1997

APPROVED FOR PUBLIC RELEASE; DISTRIBUTION UNLIMITED.

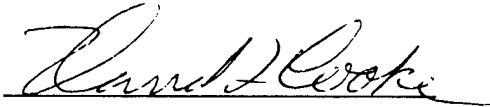
20021008 019



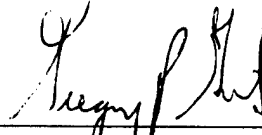
AIR FORCE RESEARCH LABORATORY  
Space Vehicles Directorate  
29 Randolph Rd  
AIR FORCE MATERIEL COMMAND  
Hanscom AFB, MA 01731-3010

---

This technical report has been reviewed and is approved for publication



DAVID L. COOKE  
Contract Manager



GREGORY P. GINET, Chief  
Space Weather Center of Excellence

Qualified requestors may obtain additional copies from the Defense Technical Information Center (DTIC). Other requests shall be referred to AFRL/VSBX.

If your address has changed, if you wish to be removed from the mailing list, or if the address is no longer employed by your organization, please notify AFRL/VSIM, 29 Randolph Road, Hanscom AFB, MA 01731-3010. This will assist us in maintaining a current mailing list.

Do not return copies of this report unless contractual obligations or notices on a specific document require that it be returned. Destroy by any means that will prevent disclosure of contents or reconstruction of this document.

REPORT DOCUMENTATION PAGE			Form Approved OMB No. 0704-0188	
Public reporting burden for this collection of information is estimated to average 1 hour per response, including the time for reviewing instructions, searching existing data sources, gathering and maintaining the data needed, and completing and reviewing the collection of information. Send comments regarding this burden estimate or any other aspect of this collection of information, including suggestions for reducing this burden, to Washington Headquarters Services, Directorate for Information Operations and Reports, 1215 Jefferson Davis Highway, Suite 1204, Arlington VA 22202-4302, and to the Office of Management and Budget, Paperwork Reduction Project (0704-0188), Washington, DC 20503.				
1. AGENCY USE ONLY (Leave blank)	2. REPORT DATE January 1998	3. REPORT TYPE AND DATES COVERED Final Report (Dec. 1991 - Dec. 1997)		
4. TITLE AND SUBTITLE  Space System-Environment Interactions Investigation		5. FUNDING NUMBERS  PE 63410F PRS327 TA 01 WU AA F19628-91-C-0187		
6. AUTHOR(S)  M. J. Mandell, G. A. Jongeward, V. A. Davis, I. Katz, R. A. Kuharski				
7. PERFORMING ORGANIZATION NAME(S) AND ADDRESS(ES) Maxwell Federal Division, Inc. Maxwell Technologies 8888 Balboa Avenue San Diego, California 92123-1506		8. PERFORMING ORGANIZATION REPORT NUMBER  MFD-DFR-98-15996		
9. SPONSORING/MONITORING AGENCY NAME(S) AND ADDRESS(ES) Air Force Research Laboratory 29 Randolph Road Hanscom AFB, MA 01731-3010 Contract Manager: Dr. David Cooke/VSBS		10. SPONSORING/MONITORING AGENCY REPORT NUMBER  AFRL-VS-HA-TR-98-0019		
11. SUPPLEMENTARY NOTES				
12a. DISTRIBUTION/AVAILABILITY STATEMENT  Approved for public release; distribution unlimited.		12b. DISTRIBUTION CODE		
13. ABSTRACT (Maximum 200 words)  This report describes work conducted for a contract to support research into the interactions of space systems with the space environment. This report covers theoretical and calculational research in support of the SPEAR 3 program using the EPSAT and DynaPAC computer codes. Analysis of CHAWS and PASP Plus flight data is discussed.				
14. SUBJECT TERMS Spacecraft, Space Environment, SPEAR, EPSAT, DynaPAC, CHAWS, PASP Plus, Solar Arrays, Wakes, Parasitic Current Collection			15. NUMBER OF PAGES	
			16. PRICE CODE	
17. SECURITY CLASSIFICATION OF REPORT UNCLASSIFIED	18. SECURITY CLASSIFICATION OF THIS PAGE UNCLASSIFIED	19. SECURITY CLASSIFICATION OF ABSTRACT UNCLASSIFIED	20. LIMITATION OF ABSTRACT SAR	

## TABLE OF CONTENTS

Section	Page
1. Introduction .....	1
2. Preflight SPEAR 3 Calculations .....	3
2.1 EPSAT Calculations in Support of Maintaining a High Apogee for SPEAR-3.....	3
2.2 DynaPAC Calculations of the SPEAR-3 Floating Potentials and Currents.....	4
2.3 DynaPAC Calculations for ESA Currents and Angles.....	5
2.4 Neutral Densities Produced by the Neutral Gas Release System.....	6
2.5 NGRS-Induced Breakdown of the SPEAR 3 Negative Body Sheath .....	8
2.6 SPEAR-3 Mockup Analysis – Floating Potential.....	15
3. Comparison of Calculations and SPEAR 3 Flight Data.....	22
3.1 Neutral Gas Effects .....	22
3.2 Magnetic Field Effects on Current Distribution .....	24
4. CHAWS Experiment Analysis.....	27
4.1 CHAWS Statistical Analysis.....	27
4.2 CHAWS in the Shuttle Wake.....	29
5. The PASP Plus Experiment .....	32
6. SPREE .....	33
7. High Power Microwave Studies.....	34
8. DynaPac .....	35
9. References .....	36

## **1. Introduction**

This is a summary of the technical work performed on contract F19628-91-C-0187 titled "Space System-Environment Interactions Investigation." A more detailed summary is presented in the interim report Mandell, Jongeward, Kuharski, and Davis, PL-TR-97-2162. The objectives of this contract are to support, with theoretical and modeling studies, research into the interactions of space systems with the space environment that are of interest to the Air Force. Work was performed in support of the SPEAR 2 and SPEAR 3 rocket flight experiments, the PASP Plus orbital experiment, the CHAWS and SPREE shuttle experiments, and the High Power Microwave Program. The work was performed by Dr. Myron J. Mandell, Dr. Gary A. Jongeward, Dr. Victoria A. Davis, Dr. Ira Katz, and Dr. Robert A. Kuharski. The publications supported by this contract are listed in Table 1.

**Table 1. Contract Publications**

1. M. J. Mandell, I. Katz, G. A. Jongeward, V. A. Davis, D. E. Parks, and D. L. Cooke, "Theoretical and Computer Modeling Support for SPEAR II," in *SPEAR II, High Power Space Insulation*, eds. H. A. Cohen and T. G. Engel, Texas Tech University Press, Lubock, Texas, 1995.
2. M. J. Mandell, T. T. Luu, J. R. Lilley, Jr., D. L. Cooke, "DynaPAC-A 3-D Finite Element Plasma Analysis Code," *Proceedings of the DNA Numerical Methods Symposium*, 1992.
3. M. J. Mandell, G. A. Jongeward, D. L. Cooke, W. J. Raitt, "Sheath Physics and Potential Mitigation on the SPEAR-III Rocket Experiment," AIAA Paper 94-0327, 1994.
4. V. A. Davis, B. M. Gardner, D. A. Guidice, P. S. Severance, "Parasitic Current Collection by PASP Plus Solar Arrays," in *Proceedings of the Fourteenth Space Photovoltaic Research and Technology Conference*, NASA Conference Publication 10180, p. 274, 1996.
5. V. A. Davis, B. M. Gardner, D. A. Guidice, "Modeling of Parasitic Current Collection by Solar Arrays in Low Earth Orbit," *Physics of Plasmas*, Vol. 3, No. 11, p. 4181, 1996.
6. V. A. Davis, B. M. Gardner, D. A. Guidice, "PASP Plus Solar Array Parasitic Current Collection Flight Results," in *Proceedings of the 31st Intersociety Energy Conversion Engineering Conference*, IEEE, Piscataway, New Jersey, p. 13, 1996.
7. M. J. Mandell, G. A. Jongeward, D. L. Cooke, W. J. Raitt, "SPEAR-3 Flight Analysis: (a) Grounding by Neutral Gas Release; (b) Magnetic Field Effects on Current Distribution", *Journal of Geophysical Research*, Vol. 103, No. A1, p. 439, 1998.
8. V. A. Davis, B. M. Gardner, D. A. Guidice, "PASP Plus Solar Array Parasitic Current Collection Flight Results", *IEEE Transactions on Plasma Science*, Vol. 26, No. 1, p. 46, 1998.
9. V. A. Davis, M. J. Mandell, D. C. Cooke, C. L. Enloe, "High-Voltage Interactions in Plasma Wakes: Simulation and Flight Measurements from the Charging Hazards and Wake Studies Experiment", submitted to the *Journal of Geophysical Research*.
10. M. J. Mandell, G. A. Jongeward, R. A. Kuharski, V. A. Davis, "Space System Environment Interactions Investigations, Scientific Report No. 1, PL-TR-96-2233.
11. M. J. Mandell, G. A. Jongeward, R. A. Kuharski, V. A. Davis, "Space System Environment Interactions Investigations, Scientific Report No. 2, PL-TR-97-2162.

## 2. Preflight SPEAR 3 Calculations

Seven studies were performed in support of SPEAR 3 experiment design. A more detailed description of the work appears in Reference 1.

### 2.1 EPSAT Calculations in Support of Maintaining a High Apogee for SPEAR-3

A study was done to evaluate the impact on the mission objectives if the apogee should fall below 300 km. The result was that the mission would be severely impacted. As shown in Figure 1, For a 300 or 350 km orbit, there is an extended period of roughly constant plasma density. For the 250 km orbit the peak density is never reached, the plasma density is usually varying fairly rapidly and the higher plasma densities occur early in the flight, when outgassing may not be complete. It is important to reach a high plasma density to avoid spontaneous breakdown.

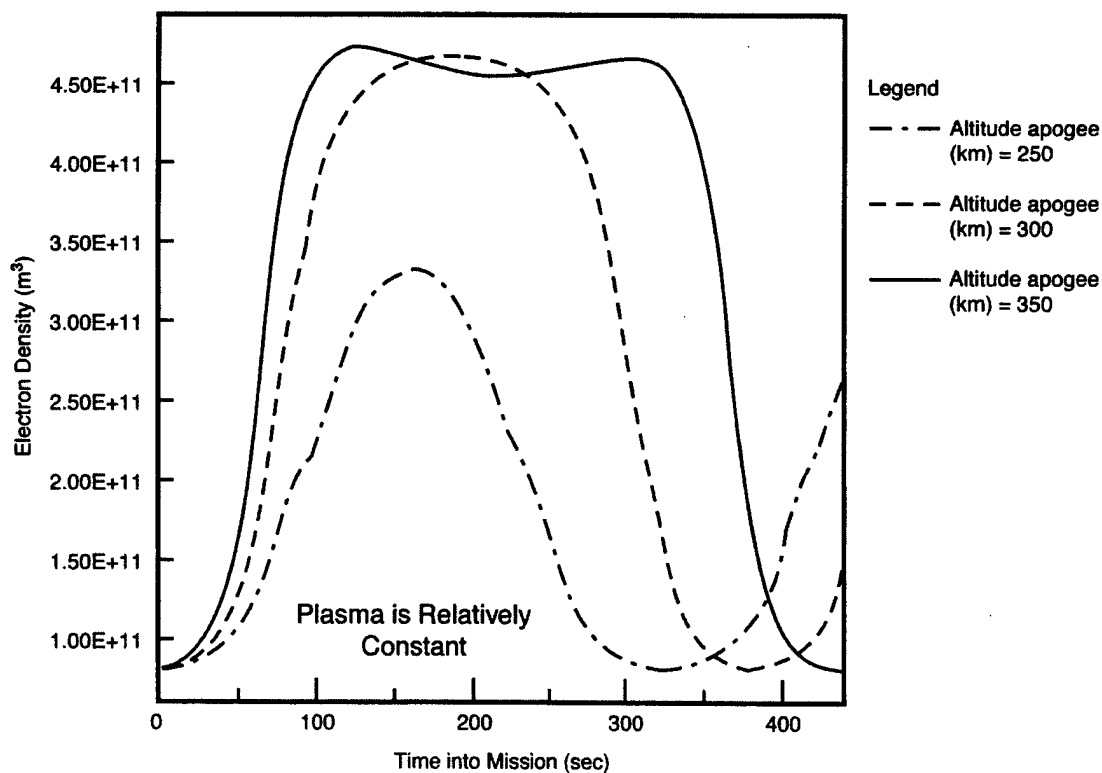


Figure 1. IRI model plasma density profiles for three SPEAR-3 orbits.

## 2.2 DynaPAC Calculations of the SPEAR-3 Floating Potentials and Currents

DynaPAC calculations of the SPEAR-3 floating potentials and currents were performed. The calculations require a three dimensional model in order to include the effects of the interaction between the sphere and body sheaths and the three-dimensional shape of the body sheath. The strictly continuous electric fields of the DynaPAC model are needed for accuracy of particle tracking.

The overlap of the sphere and body sheaths is the determining factor of the collected current. Figure 2 shows a case of wake sheath overlap. Electrons that  $E \times B$  drift along the sheath contour into the high electric field overlap region receive a waiver from the regulations of Parker and Murphy, so that they can contribute to the collected current. This effect is strongest when the magnetic field is normal to the plane of the figure (Science Attitude 1), and weakest when the magnetic field is parallel to the rocket axis (which minimizes the intersection of the drift orbits with the sheath overlap region). The collected electron current exceeds the Parker-Murphy bound for all three magnetic field orientations.

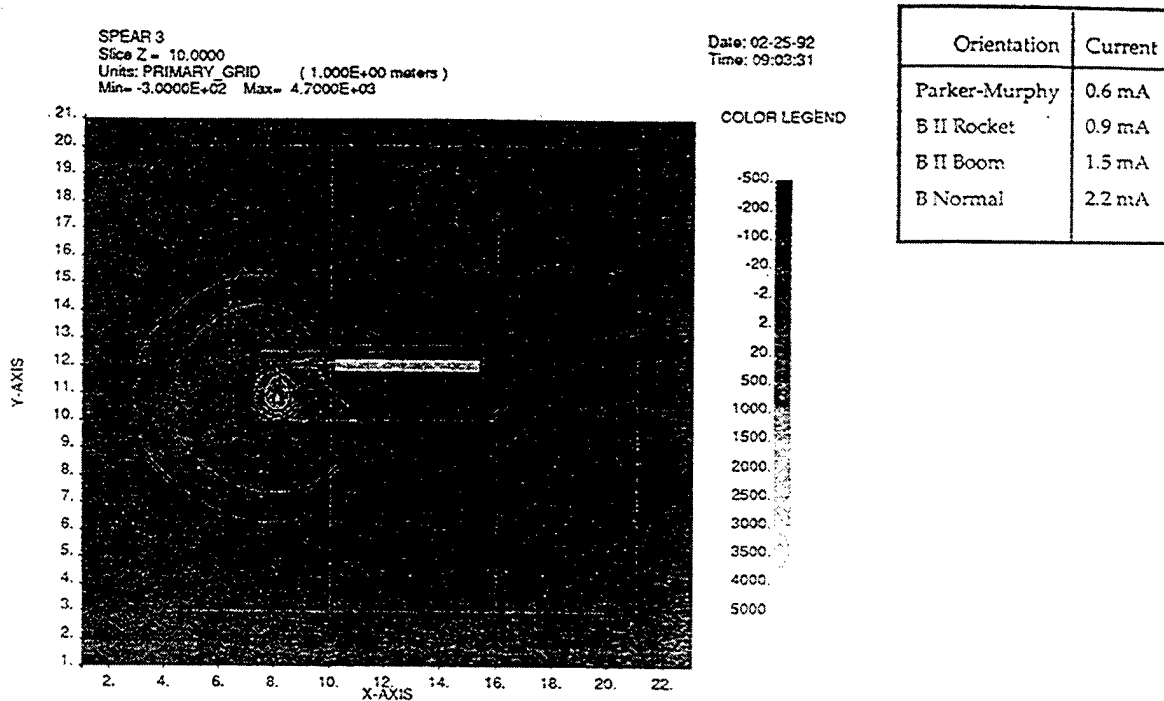


Figure 2. DynaPAC calculated electrostatic potentials about SPEAR-3, illustrating a case of weak sheath overlap.



Figure 3 illustrates the case of strong sheath overlap. Here the body sheath nearly overwhelms the sphere sheath, which is both reduced in size and partially blocked by the immense negative potential region. This reduces the collected electron current well below the Parker-Murphy bound. The highest current now occurs when the magnetic field is parallel to the rocket body, since these experience the least blockage by electrostatic barriers.

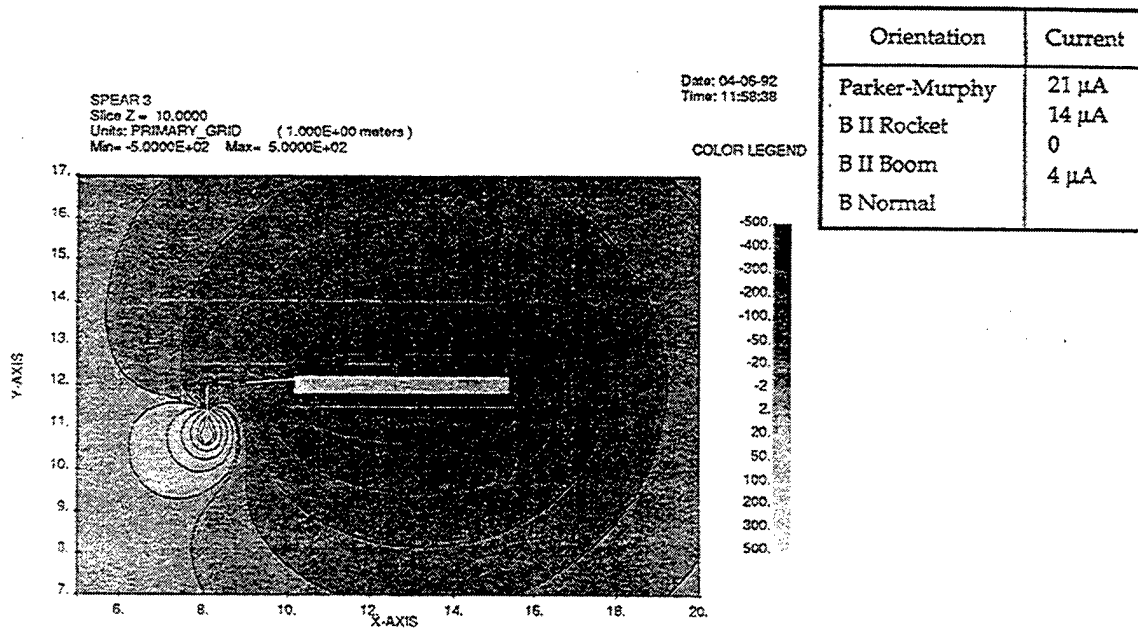


Figure 3. DynaPAC calculated electrostatic potentials about SPEAR-3, illustrating a case of strong sheath overlap.

Typically the floating potential occurs near the switch from weak to strong sheath overlap, so that there is only a weak dependence of floating potential and current on the magnetic field.

### 2.3 DynaPAC Calculations for ESA Currents and Angles

The DynaPAC calculations to determine the sheath potential were also used to determine the distribution of sheath current over the body, specifically in the region of the ESA. These calculations were used to determine the ion current and angular distribution to the detector in order to optimize the detector sensitivity.

Figure 4 shows some ion trajectories from a sheath contour. Notice that some portions of the rocket skin receive no ions, as they are totally electrostatically

Figure 4 shows some ion trajectories from a sheath contour. Notice that some portions of the rocket skin receive no ions, as they are totally electrostatically shadowed by the sphere sheath. The shadowed region typically covers nearly half of the boomward side of the rocket, and one-fourth to one-third of the side opposite the boom. The ESA is located just above the middle of the rocket on the side opposite the boom. Flux densities and incident angles were also computed.

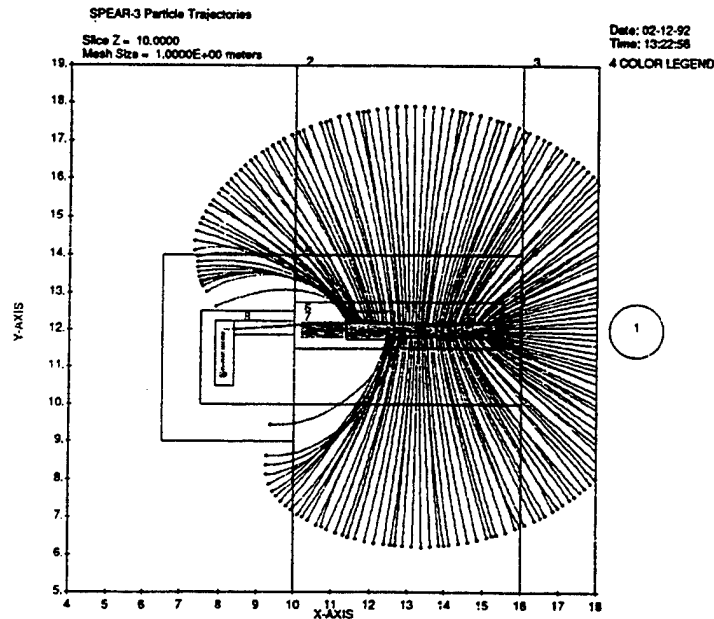


Figure 4. Typical ion trajectories from a sheath contour to the SPEAR-3 rocket body.

## 2.4 Neutral Densities Produced by the Neutral Gas Release System

The EPSAT model for nozzle plume and backflow density were used to provide neutral densities, which were used to calculate the grounding of the rocket by the neutral gas release system. The nozzle parameters used are shown in Table 2. The density near the nozzles exceeds  $10^{19} \text{ m}^{-3}$  and falls off to  $3 \times 10^{16} \text{ m}^{-3}$  near the sphere.

Table 2. Nozzle Parameters

Nozzle length	0.001
Exit radius	0.00274
Exit mach number	7
Stagnation temperature	0.0223
Stagnation pressure	$2 \times 10^6$
Throat radius	$2.685 \times 10^4$
Thrust	0.782
Area ratio	104
Number flow rate	$2.16 \times 10^{22}$
Mass flow rate	$1.005 \times 10^3$
Gamma	1.4
Species	$N_2$

Figure 5 shows the density at three positions on the rocket as a function of flow rate. The high voltage sphere appears to be safe for flow rates below ten grams per second, but the safety factor is not high. Increasing the mach number of the flow should improve the situation with regard to sphere breakdown.

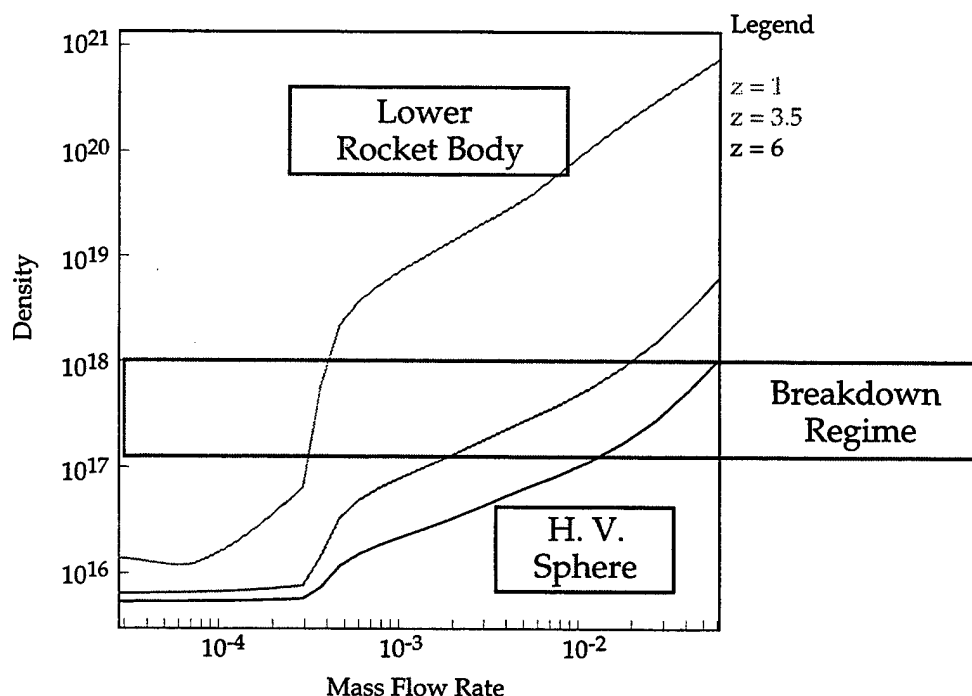


Figure 5. EPSAT-calculated neutral densities near the lower rocket body, top of rocket body, and high voltage sphere. Sphere breakdown is expected for densities above about  $10^{17} \text{ m}^{-3}$ .

## 2.5 NGRS-Induced Breakdown of the SPEAR3 Negative Body Sheath

This section describes preliminary three-dimensional considerations for NGRS-induced breakdown calculated using DynaPAC, and a dynamic, two-dimensional breakdown calculation using Gilbert. We consider the neutral species to be molecular nitrogen, although argon was actually used in the SPEAR-3 NGRS.

### 2.5.1 Three-Dimensional Considerations

Ionization breakdown for negative potentials is a two step process. An electron leaving the surface interacts with a neutral to yield an ion and an electron. The ion is accelerated back to the surface and creates secondary electrons. This process scales linearly with the neutral density. The newly created electron may interact with another neutral. Because two neutral collisions are involved, the number of secondary electrons produced as a result of second collisions scales quadratically with the neutral density. While we consider primarily the linear order processes here, higher order processes are important in achieving breakdown.

Suppose that the dominant collisions occur more than one radius from the rocket. Ionizing electrons have then been accelerated to nearly the full rocket potential, and returning ions gain this energy as well. The number of secondary electrons is proportional to the ionization cross-section for this energy times the ion-induced secondary yield.

We calculated the linear amplification process for actual SPEAR-3 potentials and nozzle densities. Electrons were tracked outward from the center of each surface cell on the rocket model. Ions were created in proportion to the ionization cross-section for the electron energy times the neutral density. The created ions were then tracked back to the rocket where they created secondary electrons. Electron energy loss mechanisms were neglected (under the assumption that the number of ions per electron would be small). Ion charge exchange was neglected (under the assumption of small neutral density).

In order to sustain breakdown, the secondary electrons must be created at the approximate location where the primary was emitted. We take this to mean the same surface cell of the DynaPAC model. Figure 6 shows the number of secondary electrons produced at the same cell as the emitted primary. The cells with substantial values are in the neighborhood of the nozzles, and face the nozzle flow direction. The maximum of this diagonal secondary production term was 0.91.

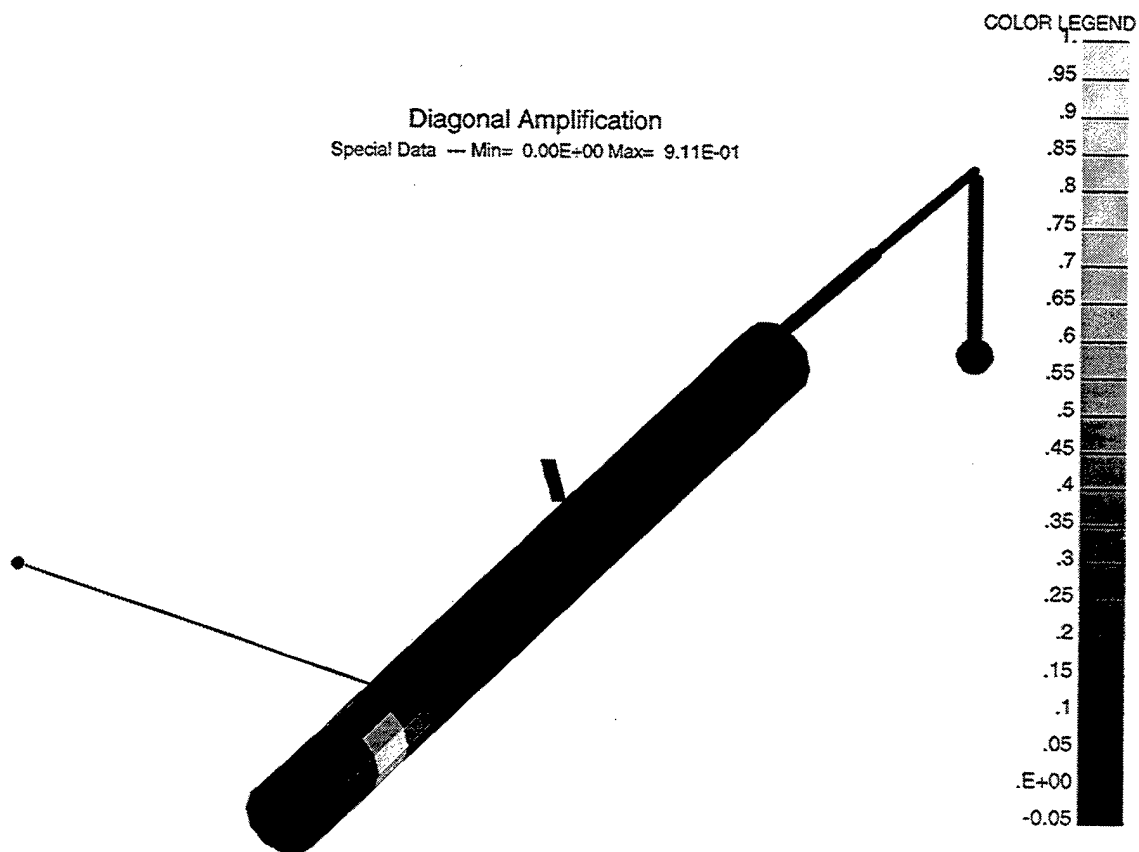


Figure 6. Secondary electron production resulting from primary electron emitted from same cell.

### 2.5.2. Two Dimensional Breakdown Calculation

Two-dimensional calculations of breakdown induced by nozzle flow were done using the Gilbert code. The rocket was represented as a sphere with radius 0.57 cm. The neutral density was obtained by taking densities corresponding to the 1 gram per second flow rate nozzle firing tangentially to the sphere, and rotating

the densities (in the plane formed by the nozzle axis and the sphere center) about the sphere diameter (passing through the nozzle). (Angle-averaging the density provided by two such nozzles gave insufficient neutral density to cause breakdown.) The neutral species was  $N_2$ . Electrons were taken with their true mass and with mass enhanced by 100, and runs were done with initial potentials of -3.5 kV and -2 kV.

Two new features were introduced for these calculations. First, an energy-dependent slowing down field (for electrons) was developed in order to reproduce the high density side of a Paschen curve. The slowing-down field is

$$E_{\text{slow}} = B N / \log (A / \sigma (\epsilon))$$

where

$$N = \text{Neutral Density [m}^{-3}\text{]}$$

$$A = 3.43 \times 10^{-20} \text{ m}^2$$

$$B = 1 \times 10^{-18} \text{ volt} \cdot \text{m}^2$$

$$\epsilon = \text{electron energy}$$

$$\sigma = \text{ionization cross-section}$$

The second improvement was to introduce an implicit algorithm (similar to those which have appeared in the literature) capable of handling very high plasma densities. The algorithm replaces Poisson's equation with

$$-\text{div} [1 + 1/2 (\omega_p (r) \delta t)^2] \text{grad } \phi = \rho_A / \epsilon_0$$

where  $\rho_A$  is the "free streaming" charge density, i.e., the charge density calculated after moving particles at constant velocity for  $\delta t$ . (The plasma frequency is also calculated using the free-streaming densities.) The algorithm consists of (1) doing the free-streaming pre-push, (2) solving for the implicit potentials, and (3) performing the actual particle push. It is not necessary to ever solve for the actual potentials. Particle deposition must be accounted for in the pre-push, but particle emission need not be done in the pre-push.

Table 3 shows the time dependence of the discharge. (Times up to 12  $\mu\text{s}$  are for real mass electrons. The heavy electron run behaved similarly, but with some

modest changes in the dynamics.) The run was started with the sphere at -3500 volts and emitting a small current of seed electrons. Significant ion return began at about two  $\mu$ s, and the ion- generated secondaries soon dominated the problem. A peak potential of -120 volts was reached but could not be sustained. The final steady state oscillated about a potential of -850 volts, with excursions of  $\pm 200$  V and a frequency of about 20 kHz.

Table 3.

Time [ $\mu$ s]	
0	Sphere at -3500 volts
2	Significant ion return current begins
6	Total space charge peaks
7	Steady ion return current of 20 mA reached
8	Peak ion space charge
9	Ion current begins to drop
9	Peak electron space charge
11	Peak secondary electron current
12	Peak potential of -120 volts
20-60	Mean ion return current of 2.5 mA
25	Total space charge has minimum
70	Equilibrium reached at -850 volts
	Mean secondary emission coefficient $\sim 0.15$
>100	Oscillations $\pm 200$ V, $\sim 20$ kHz

As we expected for the three-dimensional case, discharge was predominantly along a path passing obliquely through the nozzle plume. A quasi-neutral, dense plasma region was formed where the greatest ionization took place. Figures 7 show the electrostatic potential, ion density, and electron density during the discharge. The regions of high electron and ion density coincide, and a cathode fall region, with increased electric field, is created between the sphere surface and the quasi-neutral region.

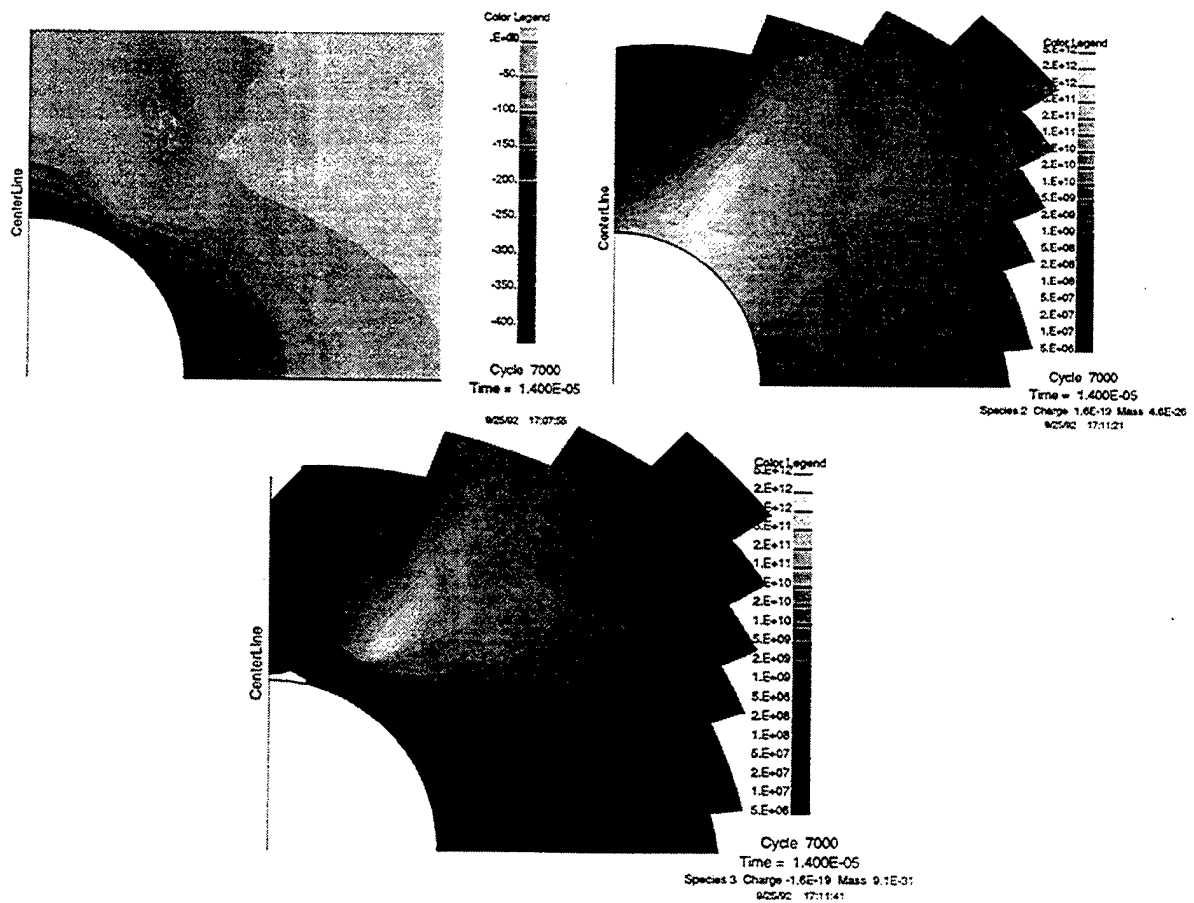


Figure 7. Plasma electron density during breakdown, showing high electron density coincident with the ion density.

### 2.5.3. Continuous Slowing Down Approximation

The importance of estimating the required gas flow for the SPEAR-3 neutral gas release system led us to pursue yet another approach to calculating breakdown in the neutral plume. This approach was to calculate the number of electron-ion pairs produced as a result of one electron emitted from the rocket and traveling a radial path (i.e., following the electric field) through the three-dimensional gas plume. The ions produced return to the rocket at low energy due to charge exchange, and thus have a secondary electron coefficient in the range 0.05 to 0.1. If their number is sufficient to reproduce the original electron by secondary emission, breakdown will occur.



Analytic formulas were fit to published cross-section and energy loss data for electron impact on neutral Argon. The ionization cross section fit is

$$\sigma(E) = 1.1 \times 10^{-16} \frac{E - 15.8}{(100 + E)^2} \text{ m}^2$$

The energy loss fit is

$$L(E) = 4 \times 10^{-16} \frac{E - 12}{100 + E} \text{ V m}^2$$

The electron macroparticles generate electron-ion pairs and loose energy independently.

Using this approach, the second Townsend coefficient was computed for radial electron paths outward from the SPEAR 3 rocket body for various flow rates. The inverse of the second Townsend coefficient for nozzle flow rates of 0.25, 1, and 2 grams per second are shown in Figure 8 as a function of direction and potential.

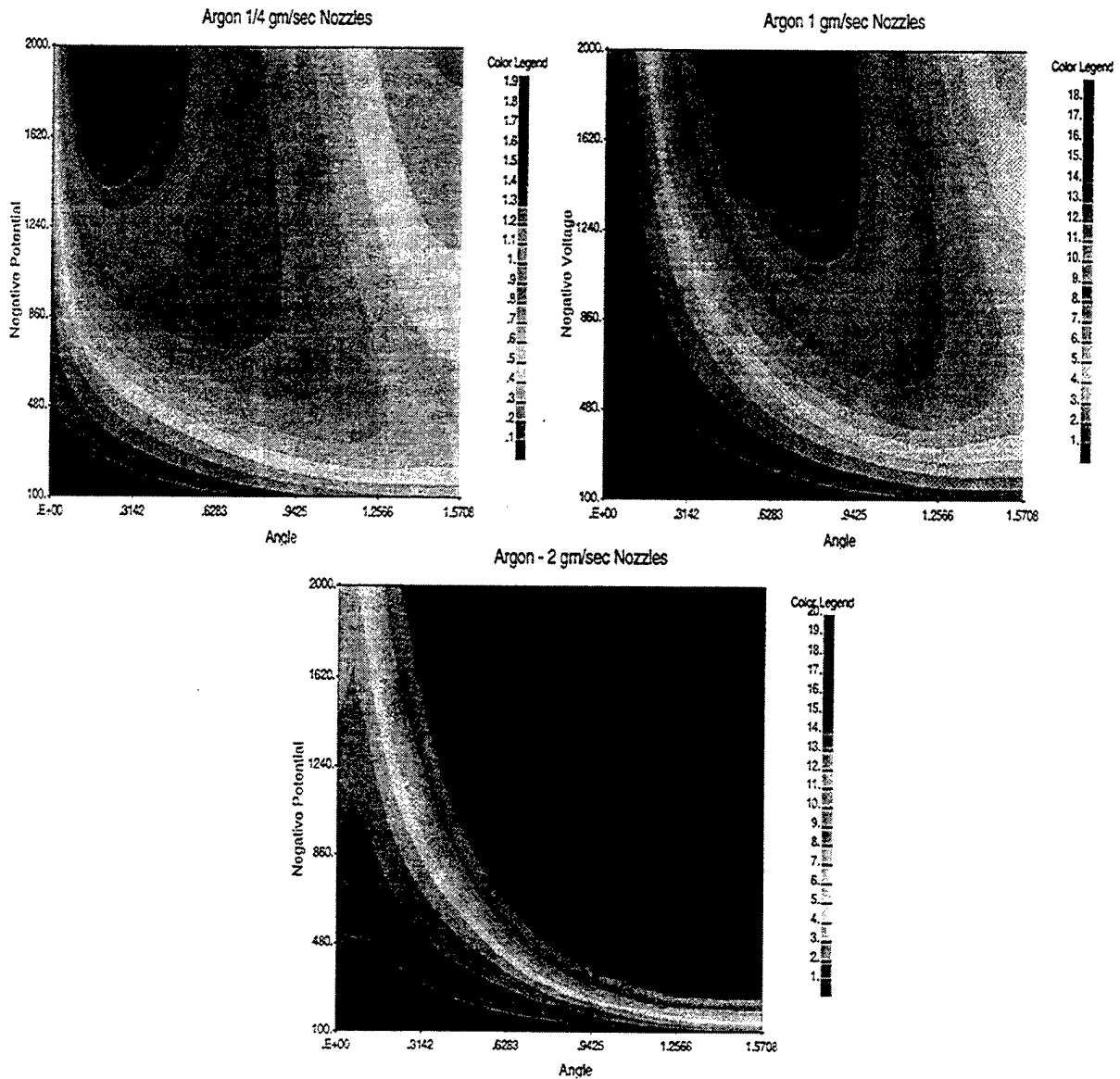


Figure 8. Inverse of the second Townsend coefficient for a nozzle flow rate of 0.25, 1, and 2 grams per second as a function of the angle from the nozzle location and the potential of the body with respect to the plasma.

The conclusions of these calculations were that (a) A nozzle flow of 2 grams per second per nozzle would be required to produce breakdown and ground the rocket. (b) During such grounding the rocket potential would be held to about 200 volts negative. (c) The breakdown path would occur 90 degrees from the nozzle location, in the direction of the gas flow.

It was strongly recommended that the flow rate be increased from the then baselined 0.5 grams per second per nozzle to 2 grams per second per nozzle. The higher flow rate was adopted by the project.

## **2.6. SPEAR-3 Mockup Analysis - Floating Potential**

DynaPAC calculations for the SPEAR-3 floating potential in space predicted that about 40 percent of the bias potential applied to the sphere would appear (in a negative sense) on the rocket body. We have confidence in these results because the same techniques were able to match the floating potential of SPEAR-I. By contrast, the floating potentials observed in the Plum Brook chamber, in the presence of plasma, were typically near 70 percent of the applied potential. To maintain confidence in the DynaPAC predictions for the space environment, we identified the factors causing the Mockup test results to be considerably more negative.

The chamber plasma density was representative of space conditions, but was considerably warmer, 1 eV rather than 0.1 eV, and had heavier ions, Argon rather than Oxygen. We can identify three effects directly leading to a more negative floating potential:

- (a) The increased ion mass directly reduces incident ion current (by a factor of 1.6), so that the model must go more negative to increase ion current and decrease electron current to meet the floating condition.
- (b) The increased ion mass also reduces the velocity of ions striking the rocket surface, resulting in lower secondary electron emission.
- (c) The increased temperature results in higher current density. Since space charge density (at a given potential) is proportional to current density times the square root of mass, the space charge is increased (relative to space) by the square root of the temperature (a factor of 3). This reduces the size of the ion sheath. The smaller ion sheath directly reduces the ion current. Even more important, the smaller ion sheath is less effective at blocking electron

flow into the sphere sheath. Both effects lead to a more negative floating potential.

Table 4 shows four DynaPAC calculations performed with only the plasma conditions changed relative to space.

Table 4.

Sphere Voltage	Body Voltage	Density	Sheath Radius	Current for B			Ion Current
				Body	Boom	Normal	
400	-800	$1 \times 10^{11}$	0.7	6.8	1.9	6.0	0.9
2000	-4000	$1 \times 10^{11}$	1.0	5.7	3.4	3.4	3.9
400	-800	$1 \times 10^{11}$	0.8	0.40	0.21	0.35	0.3
1500	-4500	$1 \times 10^{11}$	0.5	0.0	0.0	0.0	0.85

In the first three cases, the results indicate that an assumed floating potential of two-thirds negative is plausible, and this is reasonably close to the chamber results and considerably more negative than the space results. For the fourth case (which was experimentally nearly 80 percent negative), the calculation indicates a floating fraction considerably less than the assumed 75 percent. For this case (but not the other three), the ion sheath is extremely large and totally chokes off the electron sheath.

The key to the fourth case listed above is that the ion sheath exceeds the size of the chamber. The metal chamber walls serve to confine the ion sheath so that it does not choke off the electron sheath. This means that a more negative (relative to space) floating potential is needed to suppress electron collection by the sphere.

At the vacuum level achieved in the Mockup tests ( $2 \times 10^{-5}$  torr) ionization in the electron sheath can cause considerable increase in the sheath size. One-dimensional (radial) calculations show that, for parameters characteristic of the tests and realistic ionization cross-sections, ionization can roughly double the sheath radius, even if the ionization-enhancing effect of a magnetic field is neglected. The calculations indicate that the effect would be negligible if the

neutral density were a factor of four lower. This ionization effect provides yet another factor making the Mockup floating potential more negative.

Prior to installation of the "Disruptor Plate" the sphere sheath invariably broke down when high voltage was applied under plasma conditions. A DynaPAC simulation was performed to simulate the time development of the breakdown. In the simulation, a 1200 volt bias was applied to the sphere at time zero, leading to a body potential (as in vacuum) of -80 volts. The potential then developed in accordance with collection from a plasma with density  $1 \times 10^{10} \text{ m}^{-3}$ . The body collected ions in the usual way. The sphere (and boom) collected (a) electrons tracked inward (in the presence of a 0.55 gauss magnetic field) from the sphere sheath, and (b) electrons created by ionization within the sheath (collected instantly). The space charge in the sphere sheath consisted of the tracked electrons and the slowly outward moving ions created within the sheath.

Figure 9 shows the time development of the body potential, which increased roughly linearly in time to nearly -800 volts at 80 microseconds. Figure 10 shows the time development (plotted as a function of body potential) of the components of current to the rocket. The sheath electron current decreases roughly linearly as the rocket goes negative, decreasing the sphere potential. However, the rate of ion production increases nonlinearly after an initial drop. This is because the sphere sheath, which was initially fairly compact (Figure 11a) due to screening by the circulating electrons (Figure 12), is swelled by the presence of slow ions (Figure 11b).

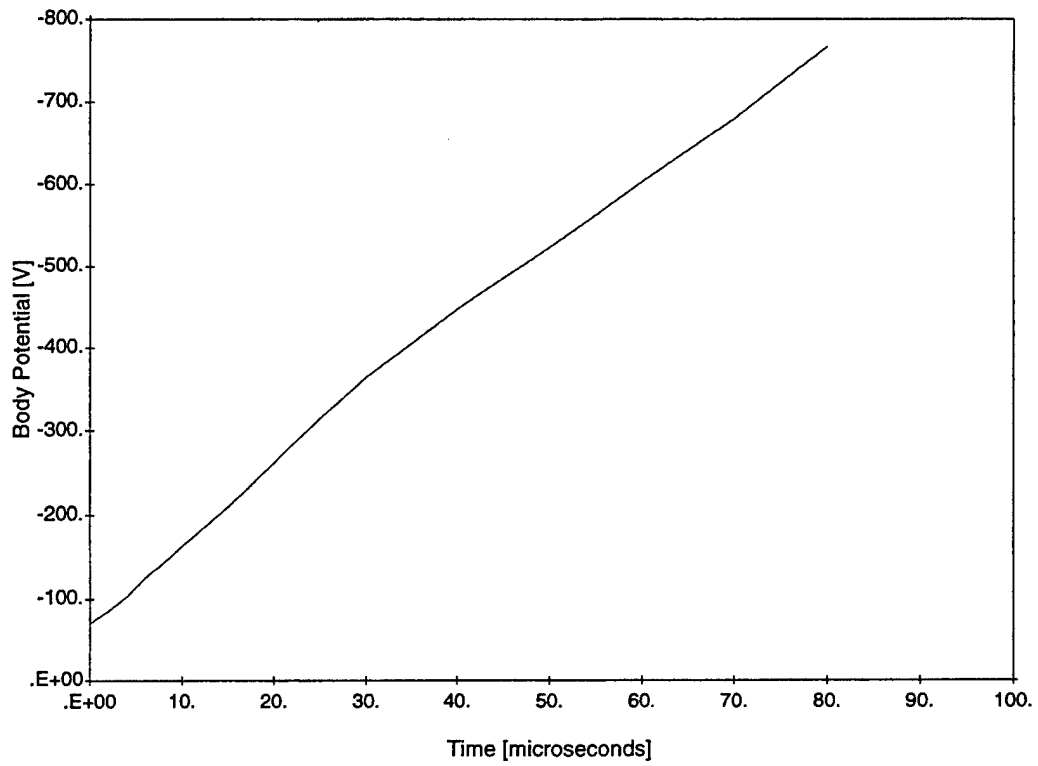


Figure 9.

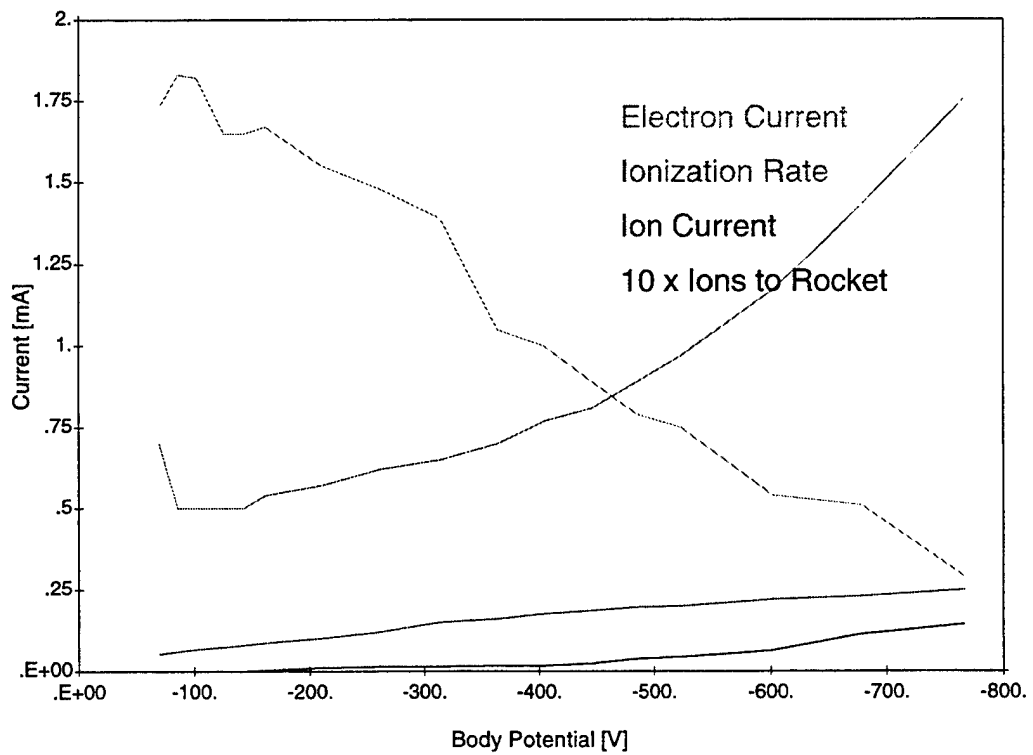


Figure 10.

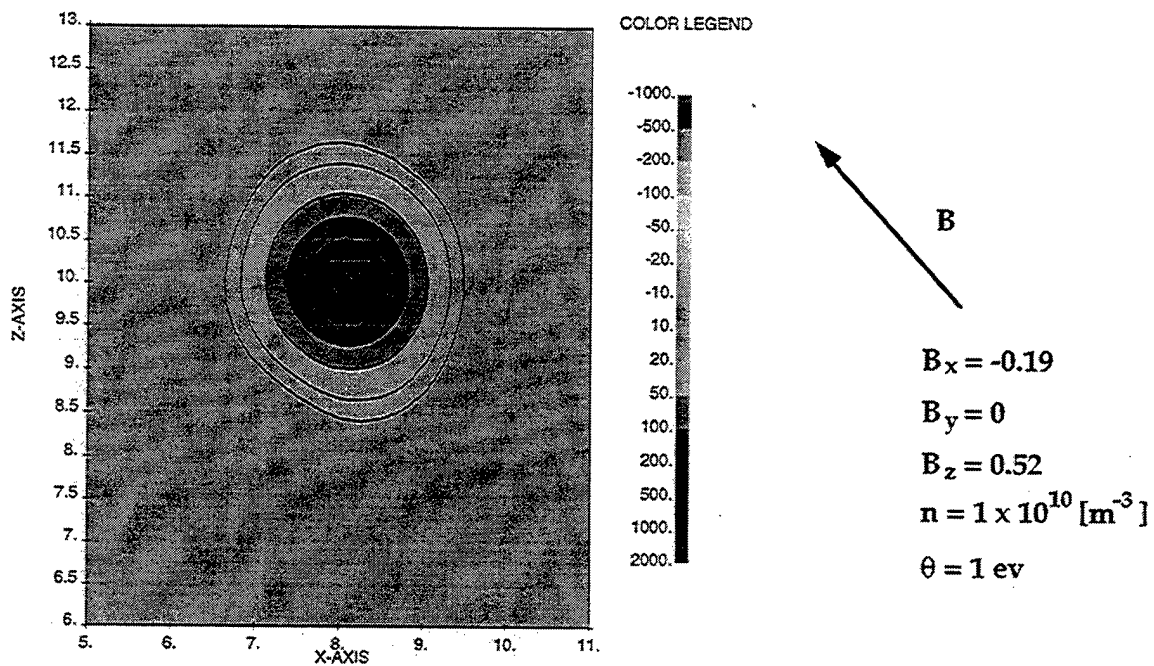


Figure 11a.

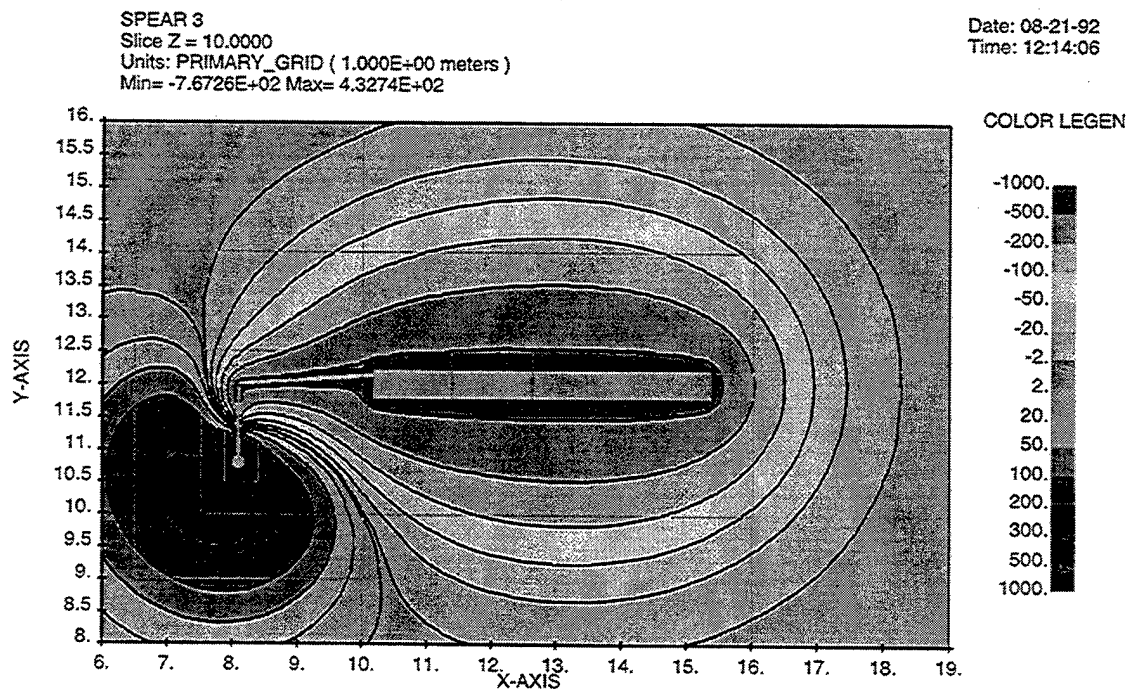


Figure 11b.

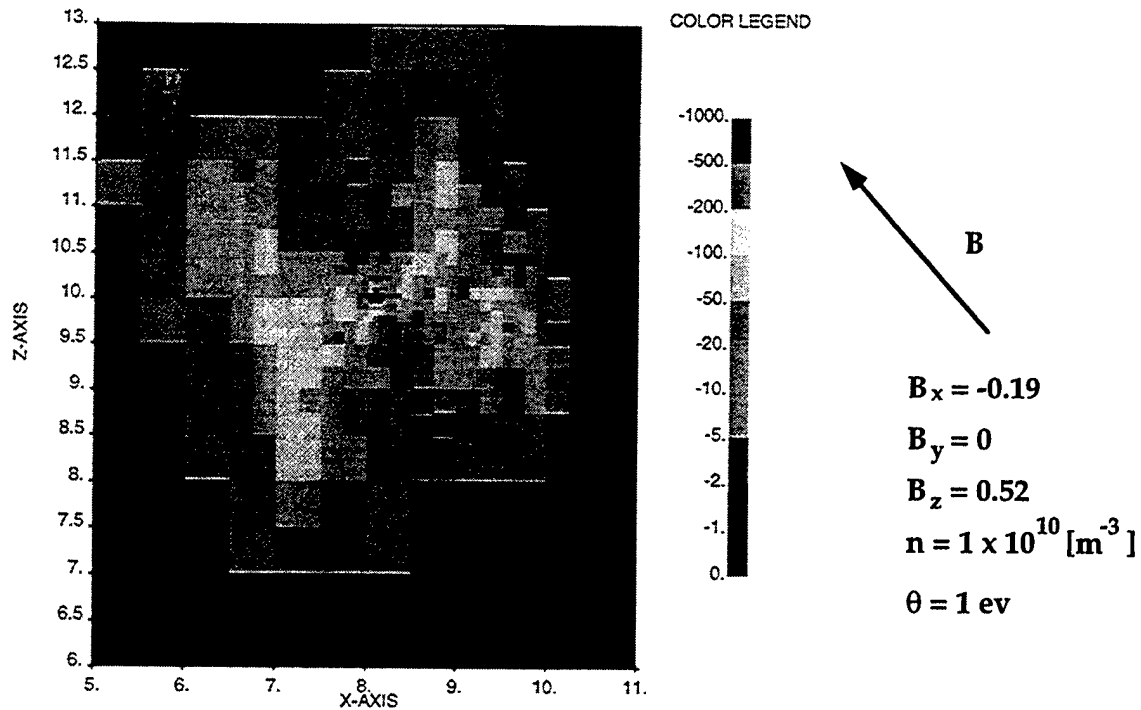


Figure 12.

While there is much to criticize about the way this calculation was done, we feel that it provides good insight into the breakdown invariably observed in the chamber. The breakdown mechanism is swelling of the sphere sheath due to ionization of the ambient neutrals by accelerated plasma electrons. If the chamber vacuum were an order of magnitude better, these breakdowns would not have taken place.

The artifice which brought success to the Mockup tests was placing a grounded "Disruptor Plate" in the path of the circulating electrons. The rationale was that electrons would no longer make many  $E \times B$  orbits, reducing the rate of ion production.

We performed DynaPAC and NASCAP/LEO calculations, with and without the disrupter plate, to examine the mechanism of discharge suppression. We were led to the conclusion that the proposed mechanism was not valid because:



- (a) Few electrons made multiple  $E \times B$  orbits in any case;
- (b) Many electron orbits missed the disrupter plate;
- (c) By Gauss's law, the total sheath electron charge could not be much affected by interruption of the  $E \times B$  orbits;
- (d) Calculations showed that the initial rate of ion production was not significantly affected by the presence of the disrupter plate.

We then proposed that the primary mechanism of discharge quenching by the disrupter plate was purely electrostatic. The plate provided a ground plane near the outer edge of the sheath, which prevented the sheath from swelling, as the ions would be neutralized by image charges on the disrupter plate. Calculations indicated that the disrupter plate reduced the effective charge of ions by about two-thirds.

We also noted that vacuum conditions were apparently better during the test series with the plate, as evidenced by improvement in the vacuum breakdown behavior of the body sheath (which cannot be attributed to the plate's presence).

We concluded that the suppression of sphere breakdown was due primarily to the electrostatic effect of the plate in preventing the sheath from swelling, secondarily to improvement in vacuum conditions, and only in a minor way to perturbation of electron orbits by the plate.

### 3. Comparison of Calculations and SPEAR 3 Flight Data

The SPEAR-3 rocket experiment was launched on 15 March 1993 to test grounding devices for negative payloads. The ability to predict floating potential and collected current for three-dimensional high voltage configurations in the space plasma environment was demonstrated on the SPEAR-I flight<sup>2</sup>. While this success was repeated for SPEAR-3, our work under this contract focused on prediction and measurement of two rather more sensitive three-dimensional phenomena: grounding of the rocket by a neutral gas plume, and the effect of the magnetic field on the distribution of collected electron current. A paper describing the work in detail will appear in *Journal of Geophysical Research*. (See Table 1.)

#### 3.1 Neutral Gas Effects

Grounding of a rocket by breakdown of a neutral gas plume had been observed accidentally on several rockets<sup>3</sup> during attitude control system (ACS) firings. Most of these observations were for rockets positively charged by electron beam emission. Sections 2.4 and 2.5 describe preflight calculations of the effectiveness of neutral gas grounding.

The gas flow rate used for neutral gas grounding was based on our preflight calculations. This gas flow rate was predicted to reduce the rocket potential to within 200 to 300 V of plasma ground. The flight data is well fit by a value of -225 V.

Figures 13 show the ESA-measured rocket potential fraction (as a function of applied potential) during gas puff shots. The rocket potential is bimodal, alternating between the no-grounding-device value and a less negative value well fit by -225 V (lower heavy gray curve in figures). This pattern holds down to applied potential values as low as 400 V. The high time resolution Floating Probe potential measurements show clearly that the low potential state is achieved immediately on the commencement of the high-rate neutral gas release, and relaxes to the higher state as the gas density decays. (The apparent long

decay time for the gas density, clearly observed by the Neutral Pressure Gauge, remains unexplained.) The low-rate gas release generally fails to reduce the rocket potential.

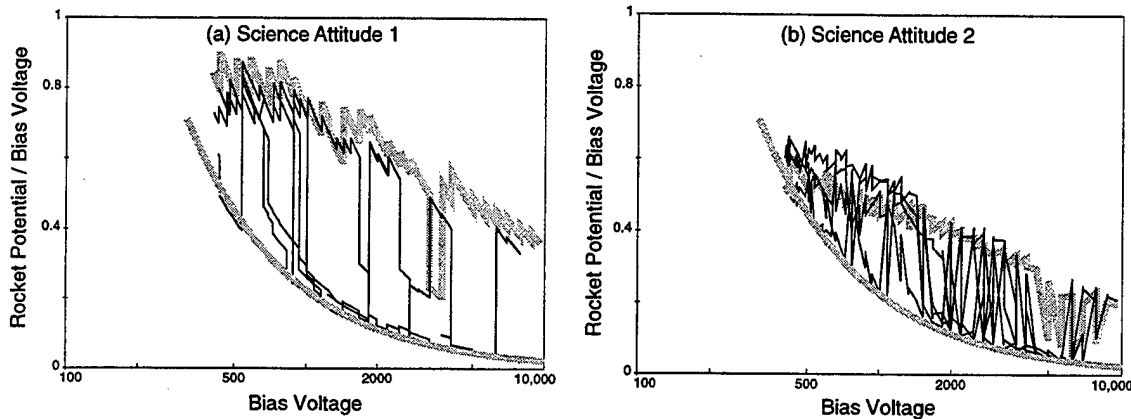


Figure 13. ESA measurements of grounding by neutral gas release (light black curves) during Science Attitude 1 (a) (shots during MET 200-215) and Science Attitude 2 (b) (shots during MET 290-305). Each figure contains one shot with no active grounding (MET 235 and MET 325, upper heavy gray curves) and four shots with intermittent gas puffs. The lower heavy gray curve on each figure corresponds to a rocket potential of  $-225$  V. The rocket potential consistently switches from the floating to the grounded curve at commencement of gas flow, and back to the floating curve when the gas has dissipated.

The value of the rocket potential in the grounded state (as well as the fact that it is a nearly constant value) is in excellent agreement with the Paschen-like breakdown calculations. This gives us some confidence that the suggested mechanism of a Paschen-like discharge through the gas plume is correct. Unfortunately, the low current level (about 10 mA) required to ground the rocket was not sufficient to produce optical emissions that would clarify the nature or location of the breakdown. Nonetheless, the SPEAR-3 experience provides a valuable knowledge base for assessing the use of gas jet grounding on future candidate missions.

### 3.2 Magnetic Field Effects on Current Distribution

As described in section 2.2, SPEAR-3 DynaPAC calculations were performed for a large number of voltage configurations and plasma densities in order to determine the expected floating potentials and plasma currents. These calculations were performed by first imposing an appropriate potential distribution on the payload surfaces, then calculating space potentials using an analytic space charge formula that ignored magnetic fields, and finally calculating electron currents by tracking sheath-generated electrons inward in the appropriate magnetic field. Here, we compare the results of these calculations with flight measurements of the division of electron current among the boom and the sphere for the two high altitude science attitudes.

In Science Attitude 1 the  $\mathbf{E} \times \mathbf{B}$  drift path of the electrons intersects the boom, which would therefore be expected to collect a substantial fraction of the total plasma electron current. In Science Attitude 2 Earth's magnetic field lies along the boom, so that it is magnetically insulated by the Earth's field and should collect much less current.

Table 5 shows a direct computational comparison of the magnetic field effect on grounded (*i.e.*, by the NGRS) and floating configurations. For the floating configuration (rocket at  $-2500$  V) we calculate a large increase in boom current for Science Attitude 1 relative to Science Attitude 2. In Science Attitude 1 the current is sufficient to cause a small but measurable (calculated at seven percent) increase in boom impedance.

Table 5. DynaPAC results for the apparent boom impedance in ungrounded (–1500 V) and grounded (–300 V) configurations for the two magnetic field attitudes.

Parameter	Value			
Plasma Density	$1 \times 10^{11} \text{m}^{-3}$			
Plasma Temperature	0.1 eV			
Magnetic Field	0.4 gauss			
Bias Voltage	5 kV			
Rocket Potential	–2500 V	–2500 V	–300 V	–300 V
Science Attitude	1	2	1	2
Total Current	3.7 mA	3.3 mA	16.2 mA	8.4 mA
Boom Current	2.2 mA	0.4 mA	10.3 mA	3.1 mA
Point of Injection	0.15 M $\Omega$	0.12 M $\Omega$	0.30 M $\Omega$	0.30 M $\Omega$
Apparent Impedance	1.07 M $\Omega$	1.01 M $\Omega$	2.6 M $\Omega$	1.23 M $\Omega$

In the grounded configuration (rocket at –300 V) the boom current increases markedly. For the Science Attitude 1 case, the boom current is so large that it is necessary to self-consistently take account of the nonlinear voltage distribution along the probe to obtain a sensible answer. The calculation predicts about a factor of two increase in impedance in Science Attitude 1 (**B** normal to rocket-boom plane), contrasted with about a twenty percent increase in Science Attitude 2 (**B** parallel to boom).

Figure 14 shows the flight results for the two cases. In Science Attitude 1 neutral gas grounding produces a 60 percent increase in apparent boom impedance relative to the already enhanced floating case, or about 80 percent relative to vacuum. By contrast, in Science Attitude 2 an increase of only about 10 percent is seen. Again, flight measurements confirm the DynaPAC predictions of a strong

magnetic field effect on the distribution of electron current to the sphere and boom.

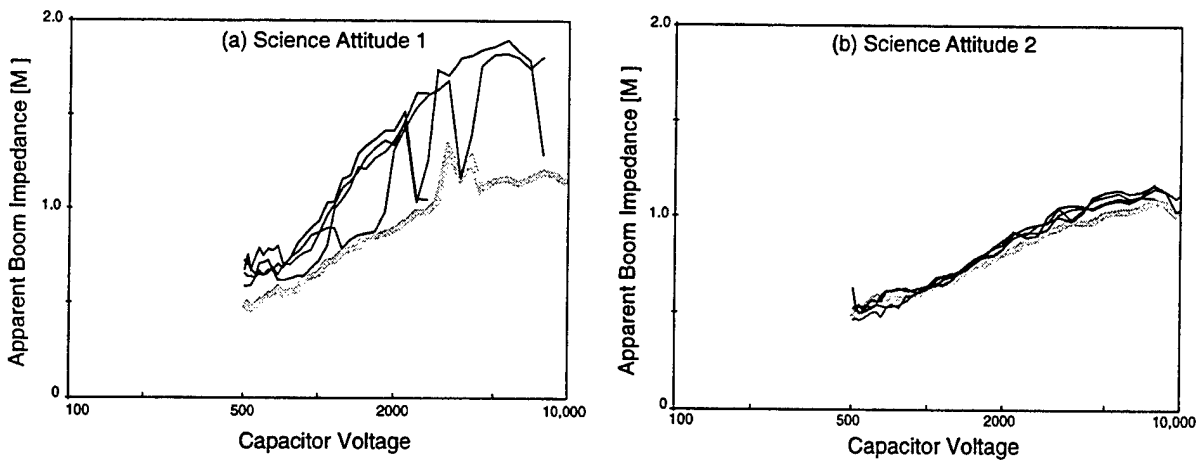


Figure 14. Measured boom impedance during shots with NGRS grounding. In Science Attitude 1, the measured impedance during grounding (MET 200-215, light lines) nearly doubles relative to the non-grounded measurement (MET 235, heavy gray line). In Science Attitude 2 (NGRS shots at MET 290-305, light lines; non-grounded shot at MET 325, heavy gray line) a much smaller effect is seen. (MET 325 is non-grounded.)

## 4. CHAWS Experiment Analysis

Under this contract, we did a statistical analysis of the CHAWS flight data and performed calculations of the current collected by the biased CHAWS probe while in the shuttle wake. We also prepared a paper that gives a complete discussion of the preflight and postflight CHAWS calculations and compares them with the results of the statistical analysis. (See Table 1.)

### 4.1 CHAWS Statistical Analysis

The current to the CHAWS wake-side probe depends on many factors. It is the unfortunate nature of space experiments that we are unable to vary each parameter while holding the others fixed. Indeed, apart from the probe bias voltage, most of these parameters are at least beyond our control, if not beyond our knowledge. Fortunately, the CHAWS data set is sufficiently large that statistical techniques can be applied to deduce the dependence on each parameter, and its relative importance.

A full discussion of the CHAWS statistical analysis is in Reference 1.

We modeled the collected current as power-law functions of applied bias,  $\phi$ , and plasma density,  $n$ , and unknown functions of tilt,  $\alpha$ , and WSF disk potential,  $\phi_d$ . For the low potential measurements photoemission is important, so that the sun-disk angle must be included:

$$I = \exp(a) \phi^b n^c \exp(d \cdot \alpha) \exp(e \cdot \phi_d) + g(\text{eclipse, sun ram angle}) \cdot 1\mu\text{A}$$

This enables us to do a linear least square fit to the form

$$\ln(I - g(\text{eclipse, sun ram angle}) \cdot 1\mu\text{A}) = a + b \cdot \ln(\phi) + c \cdot \ln(n) + d \cdot \alpha + e \cdot \phi_d$$

we choose 40 V as the dividing line between high and low potential measurements. We treat measurements made during free flight separately from measurements made while grappled by the shuttle's RMS arm. We also separate measurements made while the probe was exposed to direct ram flow (absolute

value of tilt greater than 40 degrees) or while WSF was in the wake of the Shuttle. This gives a total of six data sets.

Tables 6 and 7 show the fitting coefficients for the four wake (excluding large tilt) datasets. The coefficient of determination, which compares estimated and actual values, ranges from 0 to 1, where 1 indicates a perfect correlation. For each dataset the first column shows the results taking into account variation in all the parameters. Subsequent columns test the significance of each minor parameter by setting its coefficient to zero, thereby ignoring its variation.

Table 6. Fitting Parameters for Measurements Over 40 V.

Parameter	Grappled					Free Flight				
$\phi$	1.47	1.51	1.47	1.50	1.58	1.37	1.32	1.36	1.32	1.35
n	0.44	0.45	0.42	0.43	0	0.20	0.25	0.22	0.25	0
$\alpha$	-0.017	0	-0.018	0	0	0.027	0	0.02	0	0
$\phi_d$	-0.046	-0.051	0	0	0	0.14	0.0001	0	0	0
$\eta$	0.98	0.97	0.98	0.96	0.93	0.98	0.98	0.98	0.98	0.97

$\eta$  is the coefficient of determination



Table 7. Fitting Parameters for Measurements From 10 to 40 V.

Parameter	Grappled					Free Flight				
$\phi$	0.86	0.86	0.85	0.84	0	0.72	0.71	0.74	0.74	0.74
$n$	0.76	0.78	0.59	0.63	0.60	0.21	0.22	0.15	0.15	0
$\alpha$	-0.004	0	-0.009	0	0	0.032	0	0.040	0	0
$\phi_d$	-0.32	-0.33	0	0	0	-0.53	-0.72	0	0	0
$\eta$	0.79	0.79	0.70	0.69	0.50	0.81	0.72	0.74	0.60	0.54

$\eta$  is the coefficient of determination

#### 4.2 CHAWS in the Shuttle Wake

The resolution required to model the operations while the WSF was in the wake of the shuttle orbiter is only available with the DynaPAC compute code. Figure 15 shows the model of the WSF and the shuttle orbiter. Figure 16 shows the potentials surrounding the wake-side probe and a sampling of trajectories. Figure 17 shows the current collected by the wake side probe in the shuttle wake for three different ambient plasmas. The curve for a  $10^{11} \text{ m}^{-3}$ , 0.1 eV plasma has the same slope as the fit to the experiment. Collection from a 10% hydrogen, 90% oxygen  $10^{11} \text{ m}^{-3}$ , 0.1 eV plasma is greater, but the variation with potential is less. Results for a  $2 \times 10^{11} \text{ m}^{-3}$ , 0.1 eV plasma are closest to the flight results.

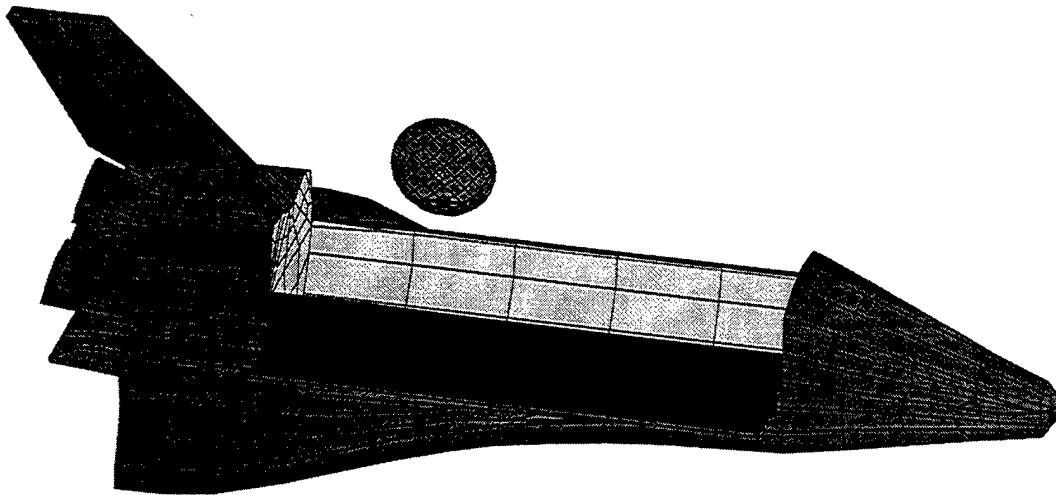


Figure 15. DynaPAC model of the WSF in shuttle wake.

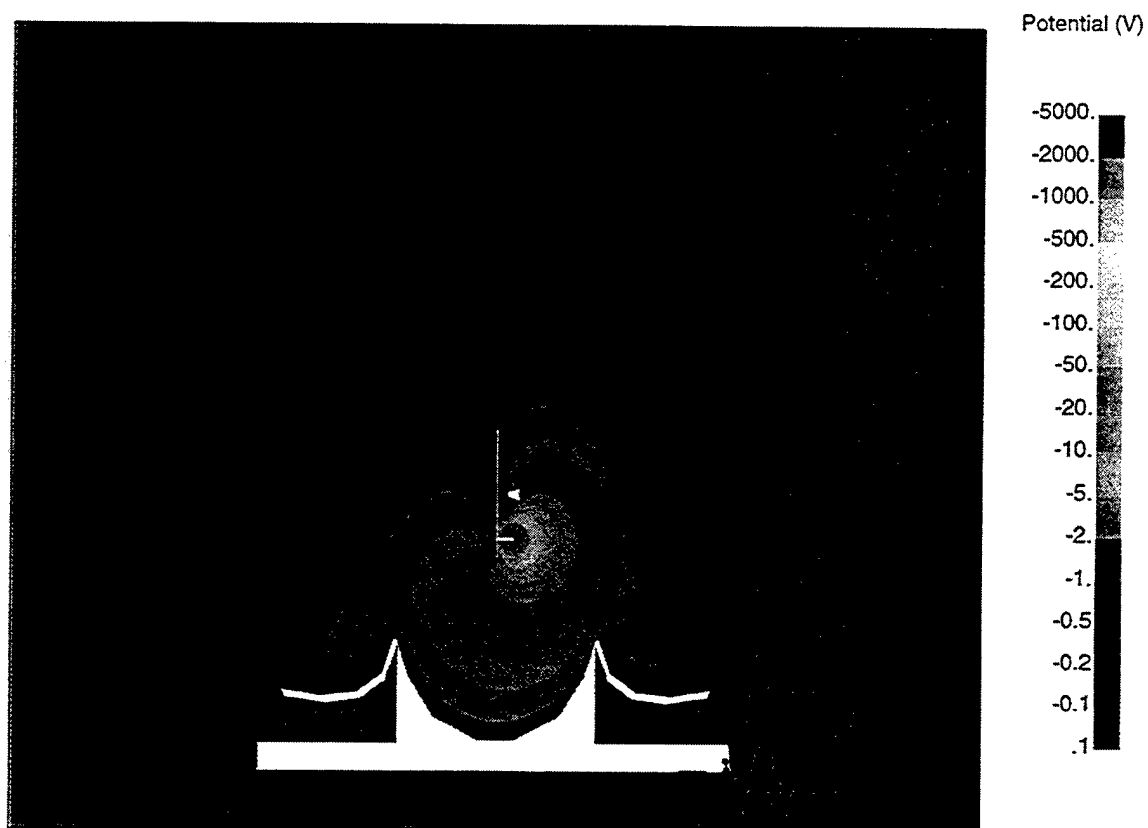


Figure 16. Potentials and sample trajectories for the WSF in the shuttle wake with the wake side probe at  $-5000$  V in a  $10^{11}$ ,  $0.1$  eV plasma, moving at  $7800$  m s $^{-1}$  as computed by DynaPAC.

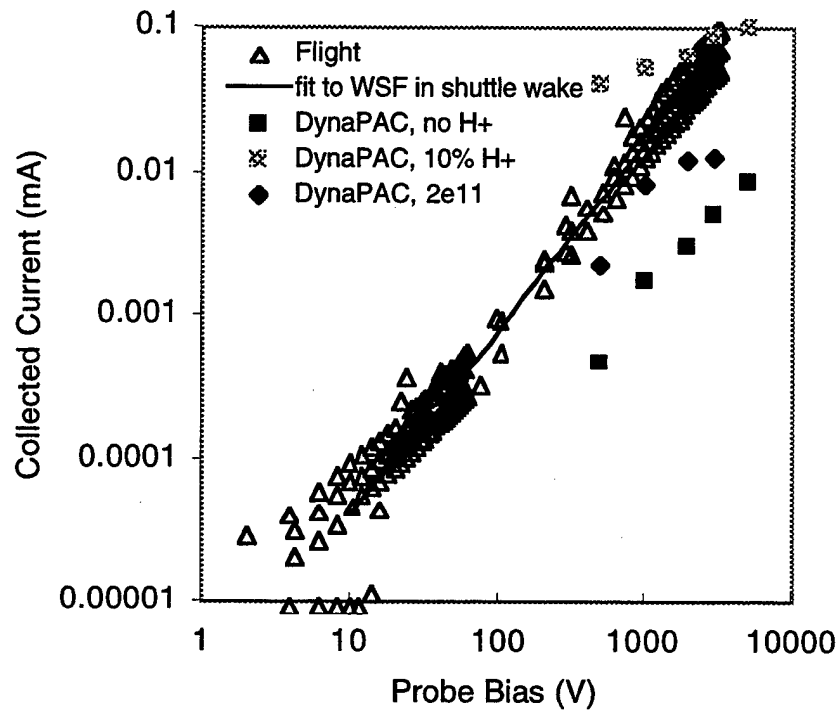


Figure 17. Wake-side probe current for WSF in the shuttle wake, as measured, from the fit, and as computed by DynaPAC for a  $10^{11} \text{ m}^{-3}$ , 0.1 eV plasma.

## **5. The PASP Plus Experiment**

Under this contract we refined the solar array current collection model developed for PASP Plus, examined ram oriented current current flight data, and examined the APEX floating potential and its influence on the current collection. We prepared several papers describing our work and compiled the PASP Plus Final Report, PL-TR-97-1013, which describes the work of the several PASP Plus researchers.

In the flight data, overall, the effective current collection area rises about two orders of magnitude as the applied bias rises one order of magnitude, as is typical when snapover plays a role. The collecting area has a weak dependence on plasma density, with larger collecting areas corresponding to lower densities (longer debye length). This dependence on plasma density is stronger for lower densities and weaker for higher densities. There is a large amount of scatter in the measurements, with the current collected under similar conditions varying by up to a factor ten. We were not able to conclusively determine the cause of this variation.

## **6. SPREE**

We created a geometric model of SPREE in the shuttle bay for the use of researchers at Hanscom Air Force Base.

## **7. High Power Microwave Studies**

We designed a system trade tool to address the basic orbital, cost, weight, and power issues associated with a possible High Power Microwave flight experiment.

## 8. DynaPAC

We made improvements in the ease of use of the Dynamic Plasma Analysis Code (DynaPAC). The code and documentation will also be delivered under this contract.

## 9. References

1. M. J. Mandell, G. A. Jongeward, R. A. Kuharski, and V. A. Davis, *Space System Environment Interactions Investigation, Scientific Report 2*, PL-TR-97-2162, 1997.
2. Katz, I., G. A. Jongeward, V. A. Davis, M. J. Mandell, R. A. Kuharski, J. R. Lilley, D. L. Cooke, R. B. Torbert, G. Larson, and D. Rau, "Structure of the Bipolar Plasma Sheath Generated by SPEAR I", *Journal of Geophysical Research* 94, 1450, 1989.
3. Gilchrist, B. E., P. M. Banks, T. Neubert, P. R. Williamson, N. B. Myers, W. J. Raitt, and S. Sasaki, "Electron Collection Enhancement Arising from Neutral Gas Jets on a Charged Vehicle in the Ionosphere", *Journal of Geophysical Research* 95, 2469, 1990.